Phosphorus, Sulfur, and Silicon and the Related Elements

ISSN: (Print) (Online) Journal homepage: https://www.tandfonline.com/loi/gpss20

Investigation of spray pyrolyzed cubic structured Cu doped SnS films

Emrah Sarica

To cite this article: Emrah Sarica (2021) Investigation of spray pyrolyzed cubic structured Cu doped SnS films, Phosphorus, Sulfur, and Silicon and the Related Elements, 196:12, 1103-1108, DOI: 10.1080/10426507.2021.1986498

To link to this article: https://doi.org/10.1080/10426507.2021.1986498

Published online: 08 Oct 2021.

PHOSPHORUS, SULFUR, AND SILICON AND THE RELATED ELEMENTS
2021, VOL. 196, NO. 12, 1103–1108
https://doi.org/10.1080/10426507.2021.1986498

Investigation of spray pyrolyzed cubic structured Cu doped SnS films

Emrah Sarica

Department of Physics, Bursa Technical University, Bursa, Turkey

ABSTRACT

Undoped and Cu doped SnS films were deposited onto glass substrates by spray pyrolysis technique in order to investigate the effect of Cu doping on their physical properties. Surface investigations showed that Cu doping reduced the surface roughness of SnS films from 36.5 to 8.8 nm. XRD studies revealed that all films have recently solved large cubic phase of SnS (π-SnS) with *a*-lattice of 11.53 Å and Cu doping led to a reduction in crystallite size from 229 to 198 Å. Additionally, all deposited films were found to be under compressive strain. Optical band gaps of SnS:Cu varied in the range of 1.83–1.90 eV. Hall-effect measurements exhibited that all films have p-type conductivity with low hole concentration ($\sim 10^{11}$–10^{12} cm^{-3}) and high electrical resistivity ($\sim 10^{4}$–10^{5} Ωcm).

ARTICLE HISTORY
Received 24 March 2021
Accepted 24 September 2021

KEYWORDS
Tin mono sulfide; copper doping; spray pyrolysis; structural properties; optical properties; surface morphology

GRAPHICAL ABSTRACT

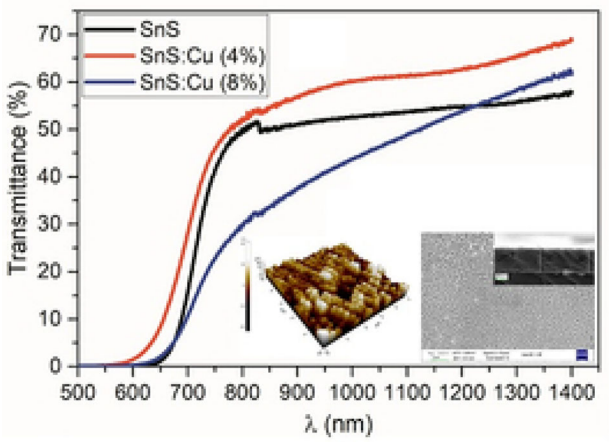

Introduction

Thin films solar cells (TFSCs) have great importance due to their low cost and competitive conversion efficiency compared to c-Si solar cells. Among these TFSCs, Cu(In,Ga)$(S,Se)_2$ (CIGS) and CdTe solar cells have high conversion efficiency (η) of over 20% and are commercially available. The highest efficiency for CIGS and CdTe-based solar cell have been reported as 23.35 and 21.0%, respectively[1]. However, the toxicity of elemental Cd and scarcity of elemental In, Ga and Te have force researchers to work on new materials which consist of environmentally friendly and abundantly elements, such as $Cu_2ZnSn(S,Se)_4$ (CZTS)[2,3]. On the other hand, its structural complexity and undesired secondary phases make it difficult to achieve high efficiency in CZTS solar cells[4]. In order to overcome the above-mentioned drawbacks, thin-film absorbers, which are binary compounds and contain inexpensive earth-abundant elements have emerged as a suitable material for solar cell applications[5].

In this context, tin mono sulfide (SnS) is a good candidate because it meets the above requirements and also possess a high absorption coefficient ($>10^4$ cm^{-1}) and suitable direct band gap ranging from ~1.3 eV (for orthorhombic structure) to ~1.7 eV (for cubic structure)[6,7]. Externally doping of thin film semiconductors is most frequently referred, as a way to tailor or improve their physical properties for photovoltaic applications. Recently, some studies have shown that doping of SnS with aluminum (Al), iron (Fe), indium (In), copper (Cu), and silver (Ag) can enhance its photovoltaic properties[8–12]. Doped and undoped SnS films can be deposited by several techniques such as RF magnetron sputtering[8], vapor transport deposition (VTD)[13], e-beam evaporation[14], thermal evaporation[15], electrodeposition[10], chemical bath depositions[7], and spray pyrolysis[12]. However, very few studies that investigate the

CONTACT Emrah Sarica saricaemrah@gmail.com, emrah.sarica@btu.edu.tr Department of Physics, Bursa Technical University, 16310 Bursa, Turkey.

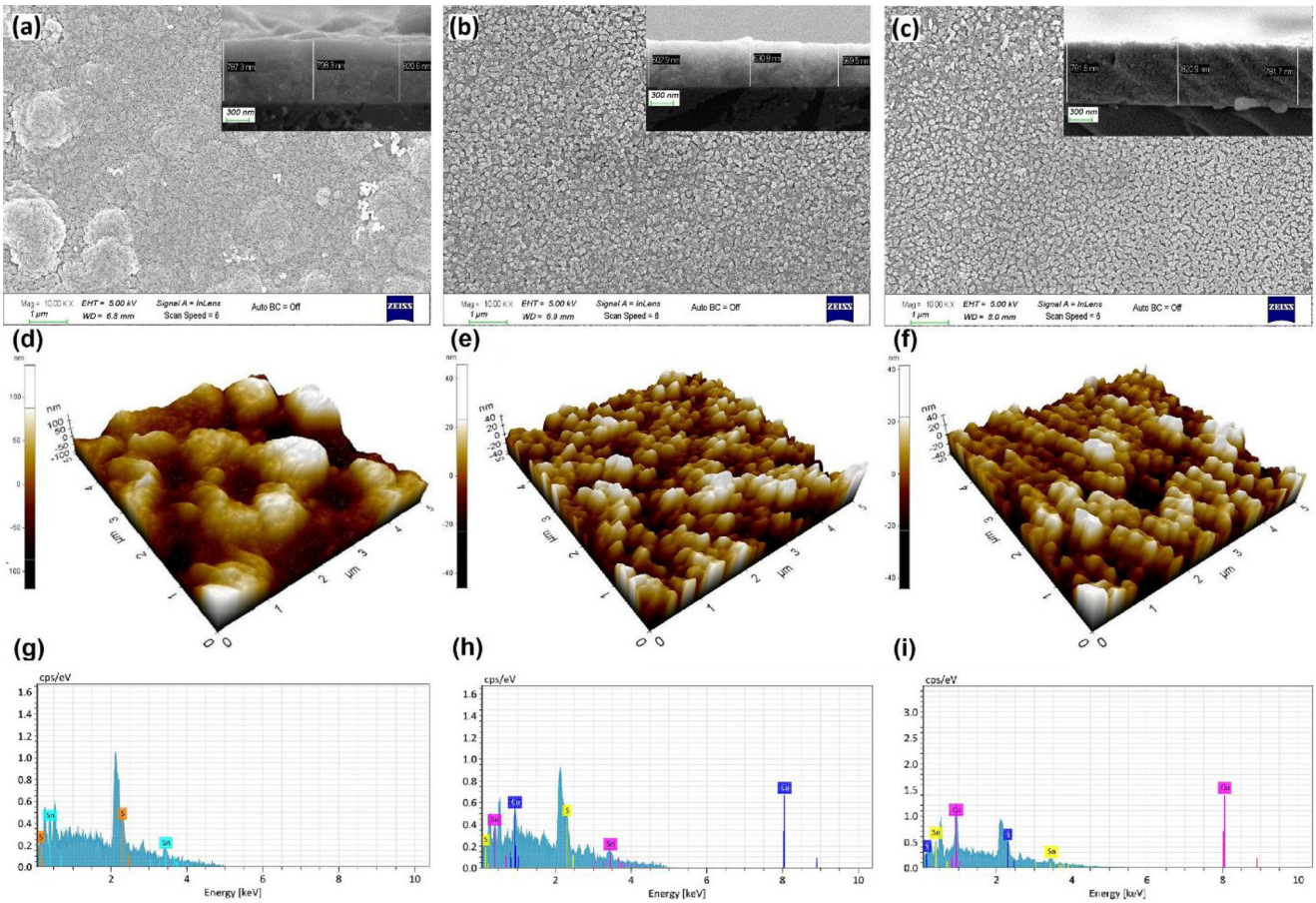

Figure 1. Surface and inserted cross-sectional SEM images of (a) undoped SnS, (b) 4%, (c) 8% Cu doped SnS films. AFM images of (d) undoped SnS (e) 4%, (f) 8% Cu doped SnS films. EDS spectra of (g) undoped SnS (h) 4%, (i) 8% Cu doped SnS films.

Table 1. Thickness (*d*), surface roughness (*R*), and elemental composition of SnS:Cu films.

			Elemental composition at%		
Material	*d* (nm)	*R* (nm)	Sn	Cu	S
SnS	800	36.5	61.93	–	38.07
SnS:Cu (%4)	600	9.3	50.09	15.13	34.78
SnS:Cu (%8)	795	8.8	41.57	26.42	32.01

effect of Cu doping on the physical properties of large cubic phase of SnS by spray pyrolysis exist in the literature. Therefore, variations in physical properties of spray pyrolyzed SnS:Cu films as a function of Cu doping concentration were investigated in this work.

Results and discussions

Morphological and elemental analysis

The SEM and AFM images were taken in order to investigate both surface morphologies and determine of film thickness. SEM images, AFM images, and EDS spectra are given in Figure 1. As seen from SEM images given in Figure 1(a–c), the film surfaces are formed homogeneously without any cracks or voids. By means of the cross-sectional images given as inset in Figure 1(a–c), the average film thicknesses were noted as 800, 600, and 795 nm for undoped, Cu doped films SnS film at 4 and 8%, respectively. Variations through the surface morpholgy of all films which were observed by AFM images given in Figure 1(d–f) were consistent with the SEM images. For undoped SnS films, agglomeration-like morphology leading to high surface roughness was noticed in AFM images as well as SEM images. These agglomeration-like structures disappeared after Cu doping and the surface roughness decreased. The average surface roughness for SnS:Cu films are listed in Table 1. Figure 1(g–i) illustrates EDS spectra of SnS:Cu films. All elements, i.e., Sn, Cu, and S were detected in these spectra and atomic percentages of these elements are listed in Table 1.

Structural analysis

XRD patterns utilized for the structural analysis are given in Figure 2. As seen from Figure 2(a), a sharp XRD peak detected at $2\theta\sim44.4^\circ$ along with some weak diffractions peaks at $2\theta\sim26.8^\circ$, 31.0°, 64.8, and° 78.0°. Moreover, it was noticed that other peaks were suppressed due to the high intensity of the peak located at ~44.4°, and suppressed peaks appeared after vertical axis was enlarged as seen from Figure 2(b). XRD patterns in Figure 2(b) were compared with both orthorhombic phase of SnS (o-SnS) given by JCPDS card No: 39-0354 and recently resolved large cubic phase of SnS (π-SnS) consisting of 64 atoms in unit cell and lattice parameters of $a = 11.5873$ Å[16–18]. As seen from Figure 2(b), XRD patterns of SnS:Cu films deposited in this study fit well with that of large cubic SnS

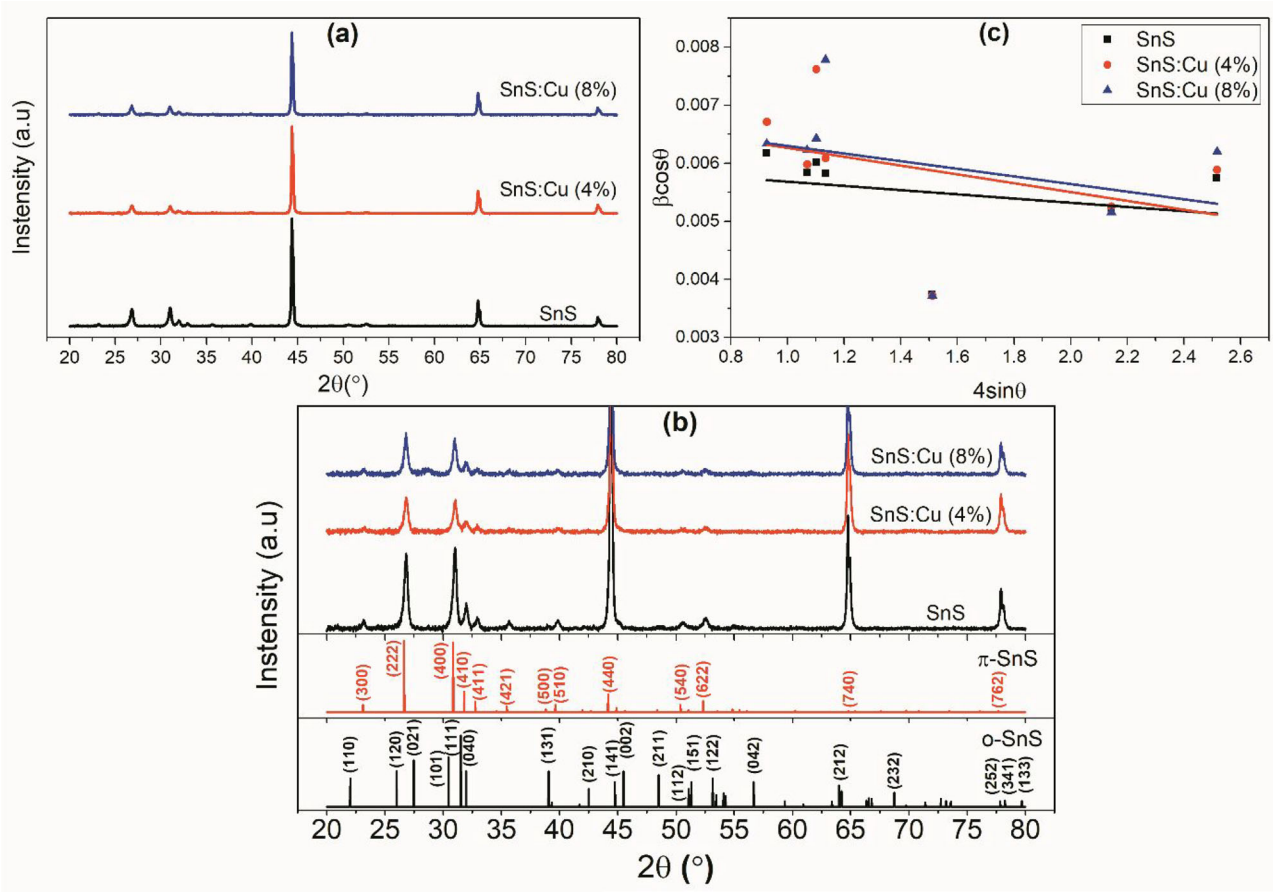

Figure 2. (a) XRD patterns of SnS:Cu films, (b) comparison of the XRD patterns with extended vertical axis with JCPDS card No: 39-0354 and Nair et al.[18], (c) W-H plots of SnS:Cu films.

phase. Accordingly, *a*-lattice parameter was calculated for all detected peaks using following equation[19] and mean values listed in Table 2.

$$\frac{1}{d^2} = \frac{h^2 + k^2 + l^2}{a^2} \quad (1)$$

By supposing that the crystallite size and strain contributions to line broadening are independent to each other, crystallite size and micro-strain values of the deposited films were evaluated in accordance with Williamson–Hall approach under a uniform deformation model[20].

$$\beta_{(hkl)} \cos\theta = \frac{K\lambda}{D} + 4\varepsilon \ \sin\theta \quad (2)$$

where β is FWHM, θ is Bragg angle, λ is wavelength of x-ray (1.54056 Å), D is crystallite size, K is shape factor, and ε is lattice distribution of micro-strain. Hence, D and ε can be extracted easily from the $\beta cos\theta$ *vs.* $4sin\theta$ plots given in Figure 2(c). D and ε values are also listed in Table 2.

As seen Table 2, the largest average crystallite size was noted as 229 Å for undoped SnS films and it decreased to 198 and 199 Å for Cu doped films SnS film at 4 and 8%, respectively. The ionic radii of Sn^{2+} and Cu^{2+} are 0.93 Å and 0.73 Å, respectively[21]. This decrease in crystallite sizes may be due to the difference in the ionic radii of the host and doping atoms. On the other hand, calculated *a*-lattice parameter is lower than the reference value $a = 11.5873$ Å, and it indicates that compressive strain on these films is expected. Compressive nature of micro-strain for Cu doped SnS films was also reported in Patel and Ray.[22] Also as seen from Table 2, variation of micro-strain has an inverse relationship with the change in crystal size.

Table 2. Peak positions (2θ), relevant plane indices (*hkl*), and full width at half maximum (FWHM) values extracted from XRD patterns and calculated average crystallite size (D), micro-strain (ε), lattice constant (a) values of SnS:Cu films.

Material	2θ (°)	(*hkl*)	FWHM (°)	D (Å)	$\varepsilon \times 10^{-4}$	a (Å)
SnS	26.80	(222)	0.3635	229	−3.63	11.537
	31.01	(400)	0.3470			
	31.99	(410)	0.3586			
	32.94	(411)	0.3485			
	44.41	(440)	0.2316			
	64.83	(740)	0.3536			
	77.99	(762)	0.4233			
SnS:Cu (%4)	26.82	(222)	0.3956	198	−7.59	11.532
	31.02	(400)	0.3557			
	31.99	(410)	0.4543			
	32.97	(411)	0.3637			
	44.43	(440)	0.2301			
	64.85	(740)	0.3566			
	78.00	(762)	0.4342			
SnS:Cu (%8)	26.81	(222)	0.3733	199	−6.57	11.537
	31.00	(400)	0.3704			
	31.98	(410)	0.3832			
	32.94	(411)	0.4652			
	44.41	(440)	0.2302			
	64.83	(740)	0.3501			
	78.01	(762)	0.4574			

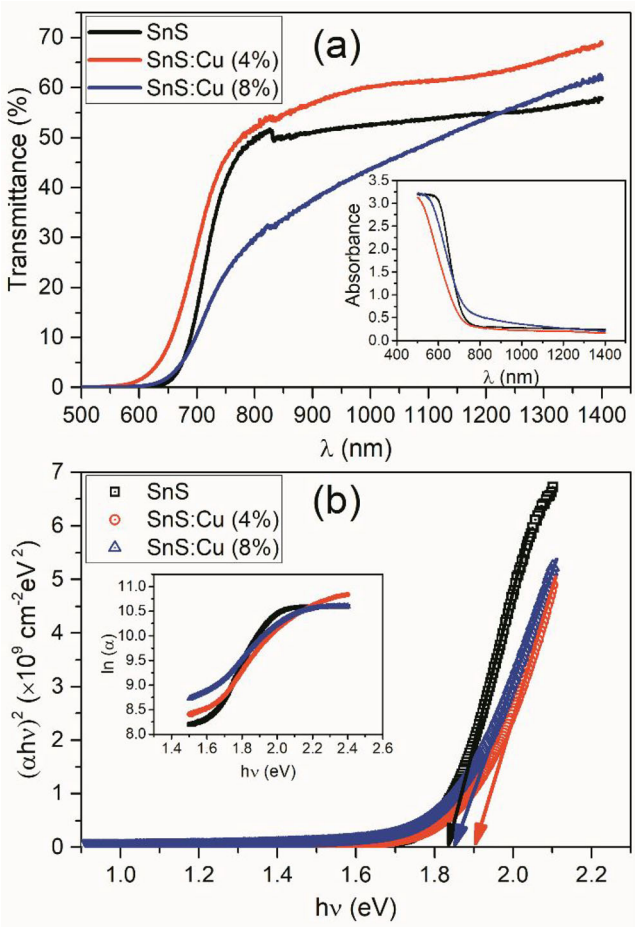

Figure 3. (a) Transmittance and absorbance (inset) spectra of SnS:Cu films and (b) Tauc plots and Inα *vs.* hν plots (inset) of SnS:Cu films.

Optical analysis

Transmittance and absorbance spectra recorded for investigation of optical properties of SnS:Cu films are given in Figure 3(a). As seen from Figure 3(a), optical transmittance is ~50%, and it increased for Cu doped films at 4% and then decreased again for Cu doped films at 8%. Transmittance of thin films tightly depends on film thickness, crystalline level, and surface homogeneity of material, so combination of these effects determines optical transmittance level[23]. Although SnS:Cu (4%) films have a worse crystallization level compared to that of undoped SnS films, the high optical transmittance may be due to their low thickness. In addition, as seen from the absorbance spectra of SnS:Cu films given as inset in Figure 3(a) fundamental absorption edge shifted toward lower wavelengths, which is the sign of broadening in optical band gaps. Optical band gaps of SnS:Cu films were determined by using $(ah\nu)^2$ *vs.* hν plots drawn according to Tauc's relation given in Equation (3) and listed in Table 3.

$$(\alpha h\nu)^2 = A\left(h\nu - E_g\right) \tag{3}$$

where E_g is the optical band gap, h is the Planck's constant, A is a constant, ν is frequency and α is the absorption coefficient calculated according to equation of $\left[\alpha = 2.303\left({}^{\text{Absorbance}}/_{d}\right)\right]$[24,25]. By extrapolating the linear part of the $(\alpha h\nu)^2$ *vs.* $h\nu$ plots to $\alpha = 0$, as given in Figure 3(b), optical band gap values of deposited films were determined as 1.83, 1.90, and 1.84 eV for SnS, SnS:Cu (4%) and SnS:Cu (8%) films, respectively. Some of studies on Cu doped SnS films which exist in the literature reported that Cu doping led to shrinkage in band gap of SnS films until the certain Cu doping concentration and enlarged for further doping concentrations, regardless of their crystal system[8,21,26,27]. Sebastian et al. and Bommireddy et al. stated that decrease in bad gap due to the increase in crystallite/grain size[21,26]. In this work, a variation in band gap may be related with the variation in crystallite size. Intentional doping of impurity atoms may generate band tails called Urbach tails which indicate the width of the localized states within the forbidden gap. Urbach energies (E_u) were determined from the slope of *ln(α) vs.* $h\nu$ plots (given in as inset in Figure 3(b)) according to Equation (4) and listed in Table 3.

Table 3. Optical band gap (E_g), Urbach energy (E_u), hole concentration (p), resistivity (ρ), and mobility (μ) values of SnS:Cu films.

Material	E_g (eV)	E_u (meV)	p ($\times 10^{11}$ cm^{-3})	ρ ($\times 10^{5}$ Ωcm)	μ (cm^2 V^{-1} s^{-1})
SnS	1.83	134	7.01	1.36	93.1
SnS:Cu (%4)	1.90	195	4.49	1.61	90.4
SnS:Cu (%8)	1.84	237	40.87	0.11	494.4

$$\alpha = \alpha_0 \exp\left({}^{h\nu}/_{E_u}\right) \tag{4}$$

where α_0 is a constant[25]. As seen from Table 3, Urbach energy values increased from 134 to 237 meV. The increase in Urbach energy implies that tail width of localized states increased due to increase in the degree of electronic disorder by Cu doping[28].

Electrical analysis

Hall-effect measurement were carried out to investigate the electrical transport properties of SnS:Cu films as a function of Cu concentration using at room temperature. Multiple measurements for each film were taken and results were averaged and then listed in Table 3. It was seen that all films have p-type conductivity with low hole concentration and high electrical resistivity. The highest hole concentration and mobility along with the lowest electrical resistivity were noted for SnS:Cu (8%) films. Such high electrical resistivity values for SnS were also reported by others[29]. However, these electrical properties are not adequate for photovoltaic applications. Especially, low hole concentration limits their utilization in solar cells as an absorber layer. Vidal et al. stated that Sn vacancies are responsible for intrinsic p-type conductivity and S-rich condition enhance hole concentration[30]. Low hole concentration in deposited SnS:Cu films in this work may be result from a sulfur deficiency in the films as seen from EDS spectra. So, loss of sulfur spray pyrolyzed SnS film may be compensated by using an excessive amount of sulfur source in the spray solution as reported[31] or annealing in a sulfur-containing atmosphere (i.e., sulphurization) and thereby hole concentration may be enhanced.

Experimental

Deposition of SnS:Cu films

First, glass substrates were cleaned by sonicating them in soapy water (after rinsing under running deionized water-DI water), acetone, methanol, and DI water, respectively. Each step took 15 min and then the glass substrates were left to dry. Following the cleaning process, SnS:Cu films were deposited onto preheated glass substrates at 350 °C by spraying a solution prepared by mixing aqueous solution of 0.05 M $SnCl_2{\cdot}2H_2O$ and CH_4N_2S. To obtain Cu doped SnS films, 0.05 M $CuCl_2{\cdot}2H_2O$ aqueous solution was added to the spray solution at ratio of 4% and 8% (v/v). The prepared spray solutions were sprayed vertically downwards for 25 min at a flow rate of 4 mL/min from a distance of 35 cm. Compressed dry air at 1.0 bar was used as carrier gas.

Characterization techniques

To perform structural investigations, X-ray diffraction (XRD) patterns were obtained in the range of $2\theta = 25°–80°$ by means of X-ray diffractometer (Bruker AXS, Discovery D8, Billerica, MA) with CuK_α radiation of $\lambda = 1.54$ Å. Surface images and cross-sectional images of SnS:Cu films were captured using scanning electron microscopy (SEM) (Carl Zeiss, Gemini 300, Jena, Germany) equipped with EDS set up in order to analyze surface properties, determine film thickness and perform elemental analysis. Additionally, Park Systems XE 100 model atomic force microscope was used to obtain the AFM images. Optical properties were studied *via* transmittance and absorbance spectra taken between wavelength range of 350–1400 nm by using a Shimadzu UV-2600 spectrophotometer (Shimadzu Corporation, Kyoto, Japan). Ecopia HMS-3000 Hall Effect measurement system equipped with 0.556 T magnets was used in Van Der Pauw geometry for determining carrier density, mobility, and resistivity of the SnS:Cu films.

Conclusion

In summary, undoped and Cu doped SnS films at 4% and 8% were deposited onto glass substrates by using spray pyrolysis technique in order to investigate Cu doping effect. AFM and SEM images showed that the surface homogeneity of SnS films improved after Cu doping and roughness decreased almost by four times. Additionally, EDS spectra revealed that all films were S-deficient. Based on structural analysis, it was reported that deposited SnS thin films have a large cubic phase with *a*-lattice ~11.53 Å and Cu doping led to reduction in crystallite size. Transmittance and absorbance spectra illustrated that absorption edge was located at between 650 and 700 nm. Calculated optical band gaps were found to be in the range of 1.83–1.90 eV. Hall-effect measurement showed that all films have p-type conductivity with low hole concentration and high electrical resistivity, which may arise due to S-deficiency and limits the utilization of spray pyrolyzed SnS:Cu films in thin film solar cells as an absorber layer. Therefore, it is proposed that excessive sulfur source may be added in spray solution or as-grown SnS:Cu films may be post-annealed in sulfur-containing atmosphere.

Disclosure statement

The author declares that he has no conflicting interests.

References

[1] Green, M. A.; Dunlop, E. D.; Hohl, -Ebinger, J.; Yoshita, M.; Kopidakis, N.; Hao, X. Solar Cell Efficiency Tables (Version 56). *Prog. Photovolt. Res. Appl.* **2020**, *28*, 629–638. DOI: 10.1002/pip.3303.

[2] Pal, K.; Singh, P.; Bhaduri, A.; Thapa, K. B. Current Challenges and Future Prospects for a Highly Efficient (>20%) Kesterite CZTS Solar Cell: A Review. *Sol. Energy Mater. Sol. Cells* **2019**, *196*, 138–156. DOI: 10.1016/j.solmat.2019.03.001.

[3] Katagiri, H.; Sasaguchi, N.; Hando, S.; Hoshino, S.; Ohashi, J.; Yokota, T. Preparation and Evaluation of Cu2ZnSnS4 Thin Films by Sulfurization of E-B Evaporated Precursors. *Sol. Energy Mater. Sol. Cells* **1997**, *49*, 407–414. [Database] DOI: 10.1016/S0927-0248(97)00119-0.

[4] Kumar, M.; Dubey, A.; Adhikari, N.; Venkatesan, S.; Qiao, Q. Strategic Review of Secondary Phases, Defects and Defect-Complexes in Kesterite CZTS–Se Solar Cells. *Energy Environ. Sci.* **2015**, *8*, 3134–3159. [Database] DOI: 10.1039/C5EE02153G.

[5] Lee, D.; Cho, J. Y.; Yun, H.-S.; Lee, D.-K.; Kim, T.; Bang, K.; Lee, Y. S.; Kim, H.-Y.; Heo, J. Vapor Transport Deposited Tin Monosulfide for Thin-Film Solar Cells: Effect of Deposition Temperature and Duration. *J. Mater. Chem. A.* **2019**, *7*, 7186–7193. DOI: 10.1039/C8TA09820D.

[6] González-Flores, V. E.; Mohan, R. N.; Ballinas-Morales, R.; Nair, M. T. S.; Nair, P. K. Thin Film Solar Cells of Chemically Deposited SnS of Cubic and Orthorhombic Structures. *Thin Solid Films* **2019**, *672*, 62–65. DOI: 10.1016/j.tsf.2018.12.044.

[7] Chalapathi, U.; Poornaprakash, B.; Park, S.-H. Chemically Deposited Cubic SnS Thin Films for Solar Cell Applications. *Sol. Energy* **2016**, *139*, 238–248. DOI: 10.1016/j.solener.2016.09.046.

[8] Baby, B. H.; Bharathi Mohan, D. Structural, Optical and Electrical Studies of DC-RF Magnetron co-Sputtered Cu, in & Ag Doped SnS Thin Films for Photovoltaic Applications. *Sol. Energy* **2019**, *194*, 61–73. DOI: 10.1016/j.solener.2019.10.049.

[9] Gedi, S.; Minnam Reddy, V. R.; Reddy Kotte, T. R.; Kim, S.-H.; Jeon, C.-W. Chemically Synthesized Ag-Doped SnS Films for PV Applications. *Ceram. Int.* **2016**, *42*, 19027–19035. DOI: 10.1016/j.ceramint.2016.09.059.

[10] Kafashan, H.; Ebrahimi-Kahrizsangi, R.; Jamali-Sheini, F.; Yousefi, R. Effect of Al Doping on the Structural and Optical Properties of Electrodeposited SnS Thin Films. *Phys. Status Solidi A.* **2016**, *213*, 1302–1308. DOI: 10.1002/pssa.201532920.

[11] Kafashan, H.; Balak, Z. Preparation and Characterization of Electrodeposited SnS: In Thin Films: Effect of in Dopant. *Spectrochim. Acta A Mol. Biomol. Spectrosc.* **2017**, *184*, 151–162. DOI: 10.1016/j.saa.2017.04.082.

[12] Sebastian, S.; Kulandaisamy, I.; Valanarasu, S.; Soundaram, N.; Paulraj, K.; Vikraman, D.; Kim, H.-S. Investigations on Fe Doped SnS Thin Films by Nebulizer Spray Pyrolysis Technique for Solar Cell Applications. *J. Mater. Sci. Mater. Electron.* **2019**, *30*, 8024–8034. DOI: 10.1007/s10854-019-01124-3.

[13] Pawar, P. S.; Cho, J. Y.; Neerugatti, K. E.; Sinha, S.; Rana, T. R.; Ahn, S.; Heo, J. Solution-Processed ZnxCd1-xS Buffer Layers for Vapor Transport-Deposited SnS Thin-Film Solar Cells: Achieving High Open-Circuit Voltage. *ACS Appl. Mater. Interfaces* **2020**, *12*, 7001–7009. DOI: 10.1021/acsami.9b14329.

[14] Hajzus, J. R.; Porter, L. M. Characterization of Electron-Beam Deposited SnS Films: Processing, Properties, and Ohmic

Contacts. *J. Vac. Sci. Technol. A* **2019**, *37*, 061504. DOI: 10.1116/1.5122785.

[15] Barman, B.; Bangera, K. V.; Shivakumar, G. K. Evaluation of Semiconducting p-Type Tin Sulfide Thin Films for Photodetector Applications. *Superlattices Microstruct.* **2019**, *133*, 106215. DOI: 10.1016/j.spmi.2019.106215.

[16] Garcia-Angelmo, A. R.; Romano-Trujillo, R.; Campos-Álvarez, J.; Gomez-Daza, O.; Nair, M. T. S.; Nair, P. K. Thin Film Solar Cell of SnS Absorber with Cubic Crystalline Structure. *Phys. Status Solidi A.* **2015**, *212*, 2332–2340. DOI: 10.1002/pssa.201532405.

[17] Abutbul, R. E.; Garcia-Angelmo, A. R.; Burshtein, Z.; Nair, M. T. S.; Nair, P. K.; Golan, Y. Crystal Structure of a Large Cubic Tin Monosulfide Polymorph: An Unraveled Puzzle. *CrystEngComm* **2016**, *18*, 5188–5194. DOI: 10.1039/C6CE00647G.

[18] Nair, P. K.; Garcia-Angelmo, A. R.; Nair, M. T. S. Cubic and Orthorhombic SnS Thin-Film Absorbers for Tin Sulfide Solar Cells. *Phys. Status Solidi A.* **2016**, *213*, 170–177. DOI: 10.1002/pssa.201532426.

[19] Cullity, B. D. *Elements of X-Ray Diffraction;* Addison-Wesley Publishing Company, Inc: Boston, MA, **1956**.

[20] Mote, V.; Purushotham, Y.; Dole, B. Williamson-Hall Analysis in Estimation of Lattice Strain in Nanometer-Sized ZnO Particles. *J. Theor. Appl. Phys.* **2012**, *6*, 6. DOI: 10.1186/2251-7235-6-6.

[21] Bommireddy, P. R.; Musalikunta, C. S.; Uppala, C.; Park, S.-H. Influence of Cu Doping on Physical Properties of Sol-Gel Processed SnS Thin Films. *Mater. Sci. Semicond. Process* **2017**, *71*, 139–144. DOI: 10.1016/j.mssp.2017.07.020.

[22] Patel, M.; Ray, A. Sputtered Cu Doped SnS Thin Films for Improved Photoelectrochemical and Heterojunction Solar Cells. *RSC Adv.* **2014**, *4*, 39343–39350. DOI: 10.1039/C4RA06219A.

[23] Kafle, B. P.; Acharya, S.; Thapa, S.; Poudel, S. Structural and Optical Properties of Fe-Doped ZnO Transparent Thin Films. *Ceram. Int.* **2016**, *42*, 1133–1139. DOI: 10.1016/j.ceramint.2015.09.042.

[24] Tauc, J.; Grigorovici, R.; Vancu, A. Optical Properties and Electronic Structure of Amorphous Germanium. *Phys. Stat. Solid* **1966**, *15*, 627–637. DOI: 10.1002/pssb.19660150224.

[25] Pankove, J. I. *Optical Processes in Semiconductors;* Courier Corporation: Chelmsford, MA, **1975**.

[26] Sebastian, S.; Kulandaisamy, I.; Valanarasu, S.; Shkir, M.; Ganesh, V.; Yahia, I. S.; Kim, H.-S.; Vikraman, D. Physical and Electrical Properties' Evaluation of SnS: Cu Thin Films. *Surf. Eng.* **2021**, *37*, 137–147. DOI: 10.1080/02670844.2020.1754623.

[27] Baby, B. H.; Thomas, A. M.; Amrutha, E. G.; Bharathi Mohan, D. Enhancement of Optoelectronic Properties *via* Substitutional Doping of Cu, in and Ag in SnS Nanorods for Thin Film Photovoltaics. *Sol. Energy* **2020**, *205*, 46–455. DOI: 10.1016/j.solener.2020.05.076.

[28] So, H. S.; Bin Hwang, S.; Jung, D. H.; Lee, H. Optical and Electrical Properties of Sn-Doped ZnO Thin Films Studied *via* Spectroscopic Ellipsometry and Hall Effect Measurements. *J. Korean Phys. Soc.* **2017**, *70*, 706–713. DOI: 10.3938/jkps.70.706.

[29] Garmim, T.; Chahib, S.; Soussi, L.; Mghaiouini, R.; El Jouad, Z.; Louardi, A.; Karzazi, O.; El Jouad, M.; Hlil, E. K.; Hartiti, B.; **et al**. Optical, Electrical and Electronic Properties of SnS Thin Films Deposited by Sol Gel Spin Coating Technique for Photovoltaic Applications. *J. Mater. Sci. Mater. Electron.* **2020**, *31*, 20730–20741. DOI: 10.1007/s10854-020-04586-y.

[30] Vidal, J.; Lany, S.; D'Avezac, M.; Zunger, A.; Zakutayev, A.; Francis, J.; Tate, J. Band-Structure, Optical Properties, and Defect Physics of the Photovoltaic Semiconductor SnS. *Appl. Phys. Lett.* **2012**, *100*, 032104. DOI: 10.1063/1.3675880.

[31] Jeganath, K.; Choudhari, N. J.; Shruthi Pai, G.; Rao, A.; Raviprakash, Y. Role of Substrate Temperature on Spray Pyrolysed Metastable π-SnS Thin Films. *Mater. Sci. Semicond. Process* **2020**, *113*, 105050. DOI: 10.1016/j.mssp.2020.105050.